


Research Article

Nanoconfined Gas Flow Behavior in Organic Shale: Wettability Effect

Shan Wu ¹, Xiaorui Wang,² Ying Yu,³ Yao Yu,³ Liang Zhang,⁴ and Ran Mao⁵

¹School of Chemical Engineering and Technology, China University of Mining and Technology, Xuzhou 221116, China

²Longdong Shale Oil Development Project Department, Changqing Oilfield Company, CNPC Qingyang, Gansu 745100, China

³No.7 Oil Production Plant of PetroChina Changqing Oilfield Branch, Gansu 745100, China

⁴Huabei Oil Communication Co. Ltd., Renqiu, Hebei 062552, China

⁵The Fourth Oil Extraction Plant of Petrochina Huabei Oilfield Company, Langfang, Hebei 065000, China

Correspondence should be addressed to Shan Wu; wushan_cumt@163.com

Received 24 March 2022; Revised 4 May 2022; Accepted 11 May 2022; Published 27 May 2022

Academic Editor: Keliu Wu

Copyright © 2022 Shan Wu et al. This is an open access article distributed under the Creative Commons Attribution License, which permits unrestricted use, distribution, and reproduction in any medium, provided the original work is properly cited.

A clear understanding of nanoconfined gas flow behavior in shale gas reservoirs is beneficial for its efficient development. Nanopores in the shale gas reservoirs are characterized by complex surface chemistry and composition, as well as affinity, while their impact on methane flow has not been investigated comprehensively before. In light of current research status, this article proposes a simple yet robust theoretical model, incorporating bulk-gas flow flux and surface diffusion of adsorption gas. In particular, wettability effect, indicating the influences of the shifted critical properties and adsorption thickness, is captured as well. In this article, gas physical attributes, such as gas compressibility factor and gas viscosity, are modified under the nanoconfinement effect and wettability effect, and also the variation of effective pore size, induced by surface wettability, is considered. Notably, wettability effect in this article is described by using a macroscopic form, surface contact angle, facilitating the model applicability. In addition, both the bulk-gas flow model and surface-diffusion model, developed in this research, are able to achieve excellent agreements compared with the existed documents, clarifying the reliability of the proposed model. Meanwhile, key role of wettability effect on nanoconfined gas flow behavior, especially for surface diffusion of adsorption gas, is demonstrated. Results show that (a) the gas flux in small nanopores may exceed that in large nanopores, due to the predominant role of surface diffusion, while pore size is less than 10 nm; (b) the absence of real gas effect will lead to inaccurate characterization of nanoconfined gas flow capacity, and the magnitude can reach 7% for pore size of 5 nm and will enlarge with further pore size shrinkage; (c) wettability effect governs the total gas flux when pore size is less than 10 nm, while its impact will be greatly mitigated when pore size is greater than 50 nm. This article provides a comprehensive investigation to shed light on surface wettability on gas flow behavior through nanopores.

1. Introduction

It is always an urgent issue to ensure the energy supply around the world, providing the basic guarantee for the development of human beings [1, 2]. Up to date, with the rapid depletion of conventional fossil energy, encompassing oil reservoirs, coal, and natural gas, some brilliant ideas are raised up to meet the increasing energy need, such as the wind energy, solar energy, and unconventional oil/gas energy [3–5]. Notably, although the unconventional oil/gas energy belongs to fossil energy, its geological reserve is

dozens greater than regular oil/gas reservoirs [6–8], presenting the favorable potential to become the alternative energy in the years to come. In this research, emphasis is put on shale gas reservoirs, a member of unconventional gas reservoirs, which are characterized by diversity of nanopores, ultralow permeability, and huge reserves. Due to its ultralow permeability, generally spanning from several to hundreds of nano-Darcy [9–11], the economic development of shale gas reservoirs was extremely challenging for a relatively long period. And, thanks to the invention of multistage hydraulic fracturing technology, a couple of high-conductivity

artificial fractures can be constructed in shale reservoirs [12, 13], dramatically advancing the gas flow capacity in the target formation. After that, the successful development of shale gas reservoirs has achieved. However, according to the typical production performance for shale gas wells, the gas production rate undergoes rapid decline at the initial production stage and then keeps stable at the middle and late stage [14–16]. From the acknowledged theory, regarding the production data analysis, the gas production rate at early stage depends on the fracture conductivity, while it heavily depends on reservoir inherent permeability at middle or late stage. Also, it should be noted that the period of middle and late production stage is far longer than the early stage. As a result, in order to have a clear image of production behavior at middle or late stage, one is supposed to have a clear knowledge of essential flow capacity in shale. However, because of the complexity exerted by nanoscale molecular interactions, the gas flow behavior in shale nanopores still remains vague. Other than that, the surface properties of nanopores [17–19], including composition, affinity, and structure, may affect microscopic interactions, further aggravating the complexity. Accordingly, precise characterization of nanoconfined gas flow behavior is helpful to explain gas production performance at middle or late production, and the motivation of this article is to address this issue.

Apart from the natural fractures, shale rock can be regarded as the nanoscale porous media. Moreover, shale matrix possesses the dual-wettability feature [20–22], including organic matter, presenting a strong attraction force on gas molecules, and the inorganic matter, presenting a strong attraction force on water molecules. It is the dual-wettability property that the gas-water distribution mode [23, 24] in shale becomes complex, as well as interesting. In the primary state, as for the organic matter in shale, due to the repulsive force exerted by organic-pore surface, the existence of water molecules in organic nanopores is hard. In addition, strength of the repulsive force will increase with the increasing thermal maturity. Notably, there exist two gas phase storage modes, including the adsorption gas, with thickness of a molecular diameter, and bulk-like gas. Also, a great deal of efforts has been devoted to investigating gas adsorption behavior [25–27], demonstrating that the adsorption phase density can be 2–5 times that of bulk-gas density. Actually, the bulk-like gas phase in the nanoscale organic nanopores is different with bulk gas, as its behavior is influenced by the interactions induced by pore surface, while the bulk gas is free of surface interactions. As a result, with the intention of capturing gas flow behavior through organic nanopores, one must shed light on the adsorption gas flow mechanism and bulk-like gas flow mechanism simultaneously. As for the inorganic nanopores, the surface mineral composition [28–30], such as quartz, feldspar, and chlorite, has strong affinity towards water molecules; therefore a thin water film takes place, with the thickness of several nanometers. The stabilization of water film in inorganic nanopores is heavily dependent on environmental humidity, pressure, and temperature, and its accurate characterization is crucial for reserve estimation and production prediction. As the adsorption positions are occupied by water molecules

in inorganic nanopores, there exists only the bulk-gas phase. From the aforementioned context, it can be inferred that the gas flow behavior in organic nanopores shows dramatic difference compared with that in inorganic nanopores; both cannot be described by regular formulas for bulk gas. In this article, we focus on gas flow behavior inside organic nanopores, consisting of bulk-like gas and adsorption gas. Nanoconfined gas flow capacity has been studied by the previous excellent contributions; the Knudsen number [31–34], defined as the ratio of mean free path to pore size, is utilized to quantify the nanoconfinement impact. When Knudsen number falls below 0.001, gas flow behavior can be characterized by the classic no-slip NS (Navier-Stokes) equation [35, 36], as the flow mechanism is continuum flow. And, the flow mechanism becomes slip flow, in which the molecules at the boundary gain mobility, when Knudsen number ranges from 0.001 to 0.1. Notably, the slip flow can also be properly described by NS equation by modifying the boundary conditions, and the parabolic relationship, in terms of the gas velocity streamline, remains valid. Applicability of the NS equation breaks down when the Knudsen number is far beyond 0.1, corresponding to the transition flow and free molecular flow. In order to cover the entire range of Knudsen number, efforts have been performed, and a series of theoretical models have been proposed. Additionally, in terms of flow mechanism of adsorption gas, the surface diffusion, a special mechanism apparently different from the above bulk-gas flow mechanisms, is considered as a suitable approach to explain the adsorption gas flow behavior. Based on the surface diffusion theory, the mobility of adsorption gas is mainly driven by concentration gradient, regarding the adsorption gas content. In light of this point, some models are proposed to describe nanoconfined gas flow in organic matter, coupling bulk-like gas flow mechanism and surface diffusion of adsorption gas. However, it remains in serious debate on the way to couple the above different flow mechanisms, and also the existence of surface diffusion in shale gas reservoirs is still questionable. Hence, the accurate characterization of gas flow capacity through organic nanopores is still challenging. Furthermore, considering the predominant role of organic matter on shale gas production performance, properly solving this issue is fairly urgent.

Multiple approaches, including molecular dynamics (MD), numerical methods (such as LBM and PNM), and theoretical models, have been applied to shed light on nanoconfined methane flow behavior. As for the MD method [37, 38], its applicability is heavily dependent on powerful computational performance, and its simulation duration is generally limited to several nanoseconds. As a result, although the MD method is well-acknowledged as the precise characterization regarding microscopic fluid behavior, it remains hard to be a frequently utilized method, due to its high expense and complex construction process of molecular systems. Using molecular dynamics, Zhang et al. investigated the impact of nanopore geometry [39], including the cylindrical and conical nanopores, on gas transport through inorganic nanopores. With the help of MD method, Sun et al. [40] constructed shale organic nanopores by utilizing kerosene molecules and studied methane flow capacity in the

constructed nanopores [41]. Yu et al. performed in-depth analysis upon gas flow characteristics by the use of MD [42], and a unified analytical model was proposed for organic and inorganic nanopores. After that, Yu et al. (2020) continued their research, and shed light on the roughness impact on nanoconfined gas flow. Wang et al. (2021) provided a comprehensive review on gas adsorption/diffusion in shale nanopores [43], highlighting the necessity of MD simulation in this research domain. In addition to MD method, LBM is a kind of numerical methods, suitable for microscopic fluid characterization. Notably, the reliability of LBM method roots in the continuum hypothesis, leading to its inherent deficiency that LBM fails to reproduce flow behavior once the Knudsen number is beyond 10 [44–46]. Zhao et al. utilized LBM method to simulate shale gas production performance, considering gas adsorption impact [47]. Due to the excellent computational efficiency, LBM method was also widely used to reveal nanoconfined water flow and nanoconfined gas-water two-phase flow. Particularly, the LBM method can serve as the promising upscaling method to link pore-scale fluid flow mechanism and that in porous media. Moreover, Huang et al. studied methane phase behavior in nanopores [48], accounting for the surface-molecule interactions as well as gas adsorption, elaborating the vapor-liquid coexistence feature. It should be highlighted that the MD and LBM method are regarded as the approaches for pore-scale fluid modeling methods, regardless of the upscaling aspect of LBM method. As a result, there exists an evident knowledge gap to characterize fluid flow in porous media. In order to address this issue properly, PNM, pore network modeling, is raised up, coupling the pore connectivity and overall conductivity [49–51]. Evidently, PNM cannot be utilized to investigate the pore-scale fluid flow behavior. Javadpour et al. reviewed gas flow models upon shale gas reservoirs, presenting the robustness of PNM describing gas flow capacity through nanoscale porous media [52]. Song et al. firstly constructed multiscale PNM in accordance with low-resolution and high-resolution SEM images, and then macroscopic parameter, permeability, was predicted by using PNM and compared with laboratory experimental results [53]. Yi et al. focused on the extraction of pore network [54], regarding shale gas samples. In particular, pore size and throat length in Yi's PNM can alter with pressure, different with existed contributions. In addition to the aforementioned methods, the theoretical model, possessing the analytical formulas and clear applicability preconditions, is also a robust approach to explore nanoconfined gas flow. Comparing with MD, LBM, or laboratory experiments, the advantage of theoretical model is free of numerical simulation complexity and measurement errors caused by apparatus. Also, formulas in the established theoretical model have clear physical meanings, facilitating the understanding of the model and subsequent modifications [55–57]. As mentioned in the above text, the shale rock, composed of organic matter and inorganic matter, is a typical dual-wettability porous media. To the current knowledge, the theoretical models have paid little attention to wettability effect on nanoconfined gas flow. Javadpour et al. revealed the existence of nanopores in shale

and proposed a theoretical model [58], combining the continuum flow and Knudsen flow, to characterize gas flow capacity in nanopores. Then, with the development success of shale gas/oil reservoirs, the theoretical investigations, in terms of fluid behavior in nanopores, become heat. The investigations can be roughly divided into two categories, the first one is modifying the boundary conditions for the slip flow [59, 60] and the other one is weight superposition of several gas flow mechanisms [61, 62]. To sum, the wettability effect has not received due attention at this point, while its impact cannot be neglected particularly at nanoscale. Hence, there is an evident knowledge gap to figure out shale gas transport behavior under wettability effect. In this article, a robust theoretical model, putting emphasis on wettability effect, is proposed, expecting to shed light on surface wettability on gas flow in organic nanopores.

The whole paper content is arranged based on the following way. At first, the physical model, presenting the organic nanopore in shale, is introduced, highlighting the wettability effect on adsorption phase and flow behavior. Then, formulas, capturing the wettability effect on shifted critical properties, the adsorption phase thickness, and the methane viscosity, are provided. Then, the formulas, describing nanoconfined flow behavior, are modified by coupling the wettability effect. As a result, the model for gas transport through the organic nanopore, considering wettability effect, is developed. The clarification upon the reliability of the proposed model is presented in Section 4. After that, concrete gas flow behavior is investigated and discussed in Section 5. Finally, several conclusions are drawn.

2. Physical Model

In this article, attempts are implemented to reveal the gas flow behavior at nanopore scale, highlighting the impact induced by surface wettability. To the current knowledge that multiple nanoconfined mechanisms have been properly addressed, the consideration of surface wettability distinguishes this research from previous contributions. Therefore, the underlying reason, for surface wettability altering gas flow capacity, is the key issue in this work. At first, the physical meaning or process, demonstrating the wettability impact, needs to be clarified. At bulk condition, in compliance with the classic theory for phase variation, the gas behavior is mainly governed by intermolecular interactions, indicating the collisions between massive gas molecules. Notably, collision between fluid molecules and surface takes place inevitably, which however can be neglected at bulk condition. Related equations of state [63–65], such as PR-EOS and RK-EOS, root in the intermolecular interactions and can reproduce bulk-fluid phase behavior with high accuracy, claiming the little impact from the surface at bulk condition. With pore size shrinkage, the space volume, available for gas molecules, undergoes reduction. As a result, the quantity, suggesting the frequency of intermolecular collisions, declines rapidly. In the meanwhile, there still exist the molecule-surface interactions, keeping nearly unchanged no matter at bulk condition or in the narrow pores. Therefore, on the basis of the above analysis content, the frequent

surface-molecule interactions in narrow pores are expected. Particularly, the surface impact may play the dominant role determining fluid behavior in nanopores. In the other words, when pore size shrinks from several micrometers, denoting the bulk condition, to nanometers, and denoting the shale nanopores in this article, the surface impact, suggesting the interaction force imposed on the gas molecules, cannot be neglected and becomes a predominant role. Thus, the evident difference between the gas behavior in bulk condition and that in the nanoconfined condition is the relative strength of the surface-molecule interactions.

Following the above analysis, it is attractive to put in-depth investigation on key factors, affecting the relative strength of surface-molecule interactions in nanopores. In this article, the surface wettability effect, generally described as the macroscopic contact angle, is the research emphasis. Although dramatic efforts are devoted to studying nanoconfined gas flow behavior, the wettability impact has not been revealed at this point. As depicted in Figure 1, the fluid distribution characteristics under diverse surface wettability are presented. Fluid molecules in nanopores can be categorized as adsorption phase, which is close to surface with a thickness of 1~3 molecular diameters [66, 67], and bulk-like phase away from the surface. As for nanopores with strong affinity, fluid molecules, belonging to adsorption phase, increase a lot, which are highlighted in green in Figure 1(a). From the left side to the right side, the adsorption molecules decline with decreasing surface affinity, as a result of the weak attraction force upon gas molecules. Therefore, the gas flow behavior will be altered due to the wettability impact; from the fluid distribution feature in Figure 1, it is evident that surface diffusion in nanopores with strong affinity will be stronger than that with weak surface affinity. Also, bulk-phase flow capacity will weaken due to the shrinkage of pore size, caused by the occupation of adsorption molecules. Accordingly, wettability effect will make a difference upon nanoconfined gas flow behavior, including both surface diffusion for adsorption molecules and bulk-like gas flow, which however has not received due attention. This article performs attempt to study this issue, focusing on gas flow capacity through organic nanopores considering different surface contact angles.

3. Model Establishment

This article focuses on the wettability effect on gas flow behavior through organic nanopores. Notably, the wettability effect is captured by coupling the shift of critical properties as well as adsorption thickness in the gas transport model. In detail, the shifted critical properties are utilized to evaluate gas viscosity and density, further affecting the bulk-like gas flow behavior. Meanwhile, the adsorption phase thickness is considered while calculating surface diffusion. Following this way, the transport model is modified by considering the wettability effect.

3.1. Wettability Effect on Shifted Critical Properties. The gas critical properties will shrink under nanoconfinement space [68, 69], inherently caused by the strong surface-molecule

interaction. Similar with pore size, the surface affinity can also change the strength of surface-molecule interaction, as depicted in Figure 1. As a result, the critical property can be correlated with surface wettability. Feng et al. proposed a simple formula [70], elaborating the relationship between surface contact angle, macroscopic form of surface wettability, and fluid critical properties. Reliability of the formula is verified well, as it can reproduce nanoconfined fluid critical properties and achieve excellent match against experimental data or simulation results. Also, the formula demonstrates that the methane critical property, including critical temperature and pressure, can be described as a function of pore size and surface contact angle. Also, Feng et al. (2021) pointed out that nanopore geometry is also an influential factor upon critical properties, suggesting the decreasing degree of critical properties in the cylindrical nanopores will be severer than that in slit nanopores.

$$\frac{T_{cb} - T_c}{T_{cb}} = \frac{P_{cb} - P_c}{P_{cb}} = \frac{\xi}{m} \times 0.65 \ln \left(\frac{180}{\theta} \right), \quad (1)$$

where T_{cb} and P_{cb} are methane critical temperature and critical pressure at bulk state, respectively; T_c and P_c are nanoconfined critical temperature and critical pressure, respectively; θ denotes the surface contact angle, degree; ξ is a constant, related to nanopore geometry, which is equal to 0.56 for cylindrical nanopores; and m denotes the representative pore size, defined as the ratio of realistic pore radius to methane molecular diameter.

It can be inferred from Equation (1) that methane critical properties are correlated with pore size and surface contact angle at the same time. In addition, in the case of the large m , indicating that the pore size is far beyond methane diameter, the nanoconfined critical properties will approach the bulk value, regardless of the wettability impact. Notably, the wettability effect, in terms of the critical properties, becomes evident once the pore size decreases into nanoscale. As a result, it highlights the urgency to consider the wettability effect when investigating nanoconfined methane behavior. Based on Equation (1), nanoconfined methane critical properties can be calculated over a wide range of pore size and surface contact angle.

3.2. Adsorption Methane Thickness. In this article, we put emphasis on the organic nanopores in shale, inherently possessing the attraction force on methane molecules. Thus, unlike bulk-state methane molecules, freely distributed in space, the adsorption phenomenon, indicating methane molecules adhering on the surface, takes place in nanopores. In this way, the molecules in nanopores are divided into two categories, involving of the adsorption phase and bulk-like phase. The adsorption phase will inevitably occupy the space close to the surface, leading to the decline of effective pore size. Thus, the adsorption phase thickness is the key parameter, requiring to be quantified. In the meantime, there are different transport mechanisms for adsorption phase and bulk-like methane; therefore, the quantification of adsorption thickness contributes to the model establishment for gas transport through organic nanopores.

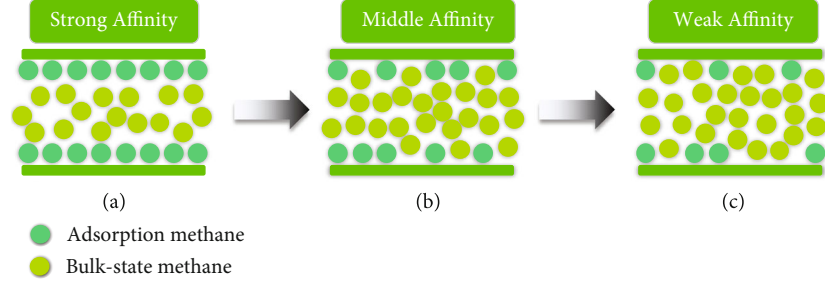


FIGURE 1: Fluid molecular distribution and flow characteristics: (a) Strong affinity; (b) Middle affinity; (c) Weak affinity.

Zhang et al. developed a robust correlation formula to characterize the adsorption thickness in nanopores [71]; its applicability covers the majority of common fluids, including methane, carbon dioxide, and oil with carbon number ranging from 3 to 10. The formula suggests that the adsorption phase thickness is not only related to the inherent molecular size, but also the pore size. The decrease of pore size will result in strong attraction force, induced by surface, upon molecules, further leading to the climb of adsorption thickness. Concrete correlation formula is given below.

$$h_{ad} = \frac{\chi}{\ln(r/\sigma)} + \delta \cdot \frac{\sigma}{r}, \quad (2)$$

where h_{ad} denotes the adsorption phase thickness, m; χ and δ denote the empirical coefficients for the correlation, dimensionless; r denotes the nanopore radius, m; and σ denotes the molecular diameter, and it equals to 0.38 nm for methane.

$$\chi = -8.314 \times 10^{-14} M^2 + 2.047 \times 10^{-11} M + 3.086 \times 10^{-11}, \quad (3)$$

$$\delta = -6.3565 \times 10^{-14} M^2 + 3.1550 \times 10^{-11} M - 5.8538 \times 10^{-10}, \quad (4)$$

where M is the methane molecular weight per mol, which is 16 g/mol here.

Notably, the formula fails to capture the wettability impact on adsorption thickness. Inferred from Equation (1), the methane phase behavior will be fairly close to the nanoconfined methane once the surface contact angle approaches 180° , indicating that adsorption phenomenon disappears at a super-weak surface affinity condition. In the other words, the adsorption thickness tends to decline with increasing surface contact angle and becomes zero when contact angle reaches 180° . However, the formula for the adsorption thickness at this point cannot reproduce the above scenario, evidently conflict with the Equation (1) and its underlying simulation results, experimental observations. In this regard, we correlate the model, raised by Zhang

et al. (2019), with the wettability impact, characterized by surface contact angle.

$$h_{ad} = \left(\frac{\chi}{\ln(r/\sigma)} + \delta \cdot \frac{\sigma}{r} \right) \times \left(1 - \frac{\theta}{180} \right), \quad (5)$$

where θ denotes the surface contact angle, degree.

On the basis of Equation (5), the decline relationship between the surface wettability and adsorption phase thickness can be captured, which keeps in compliance with Equation (1). Therefore, the theoretical background of Equation (5) is more solid than the original Equation (2), suffering the deficiency of not considering the surface wettability impact. Notably, the correlation of wettability on adsorption thickness indeed lacks necessary verification efforts and may produce uncertainty. Also, as mentioned above, consideration of wettability impact in this article is the first attempt to the knowledge, and the developed formula can capture the general variation principle between the surface contact angle and adsorption phenomenon. Thus, although Equation (5) fails to achieve the accurate characterization of adsorption thickness, it has fairly solid scientific basis and is suitable for investigation and discussion at the primary stage. It is important to admit that this technical part may result in error, and some improvements are urgent in the future. Due to the existence of adsorption phase thickness, the effective pore size for bulk-gas flow becomes the primary pore size subtracting the adsorption thickness.

$$r_{eff} = r - h_{ad}. \quad (6)$$

3.3. Bulk-Gas Flow Behavior. Gas flow capacity in the organic nanopore is contributed by two parts, involving of the bulk-gas flow and surface diffusion of adsorption molecules. In terms of the first part, bulk-gas flow behavior is closely related to the Knudsen number, characterizing the frequency of fluid-surface collisions, which is defined as the ratio of mean free path to nanopore radius.

$$Kn = \frac{\lambda}{r_{eff}}, \quad (7)$$

where Kn denotes the Knudsen number, dimensionless and λ denotes the gas free path, nm. Notably, the free path is

heavily dependent on gas viscosity [72, 73], which has the following calculation formula.

$$\lambda = \frac{\mu}{P} \sqrt{\frac{\pi ZRT}{2M}}, \quad (8)$$

where μ denotes the gas viscosity, cp; Z denotes the gas compressibility, dimensionless; R denotes the gas universal constant, which is equal to 8.314 J/mol/K; and P denotes the surrounding pressure, Pa.

The gas viscosity can be described as a function of pressure and temperature, and its change law is well characterized by the following equation [74].

$$\mu = \mu_{atm} \left[1 + \frac{A_1}{T_r^5} \left(\frac{P_r^4}{T_r^{20} + P_r^4} \right) + A_2 \left(\frac{P_r}{T_r} \right)^2 + A_3 \left(\frac{P_r}{T_r} \right) \right], \quad (9)$$

$$P_r = \frac{P}{P_c}, \quad (10)$$

$$T_r = \frac{T}{T_c}, \quad (11)$$

where λ_{atm} denotes the gas viscosity at the standard condition, suggesting the temperature is 293 K and pressure is 0.1 MPa; P_r and T_r denote the reduced pressure and reduced temperature, respectively; and A_1 , A_2 , and A_3 are empirical coefficients, which are assigned as 7.9, 9.0×10^{-6} , and 0.28, respectively.

Inferred from Equations (9)~(11), in terms of the calculation of gas viscosity, the dependence on methane critical properties is demonstrated. The methane critical properties, including T_c and P_c , are altered under the nanoconfinement effect and wettability impact simultaneously, as described in Section 3.1, and the methane viscosity is also affected by wettability effect. Therefore, the critical properties, utilized for the calculation of gas viscosity, are the nanoconfined critical properties in Equation (1), instead of that in bulk state. In this way, the gas viscosity under the wettability impact can be calculated.

Utilizing the simulation tool as well as theoretical analysis, Karniadakis et al. [75] developed a robust formula for gas transport through cylindrical nanopores [75], covering the Knudsen number over 10; however, the wettability impact has not been considered. Thus, the model, proposed by Karniadakis et al. [75], can be regarded as a desirable start point and will become a more powerful investigation approach to explore microscopic gas behavior, by taking care of the wettability impact. Also, on the basis of Wu et al. [76], the Knudsen number for typical shale gas reservoirs ranges from 0.0002 to 6 and, therefore, falls in the application scope of Karniadakis et al. [75] research.

$$J_{bulk} = \frac{r_{eff}^2 PM}{8\mu RT} (1 + \alpha Kn) \left(1 + \frac{4Kn}{1 - bKn} \right) \frac{dP}{dl}, \quad (12)$$

$$\alpha = \alpha_o \frac{2}{\pi} \tan^{-1} \left(\alpha_1 Kn^\beta \right), \quad (13)$$

where J_{bulk} denotes the gas mass flux through the nanopore, kg/m²/s; b is the empirical coefficient, dependent on the boundary condition, which is assigned as -1 in this article; and α_o , α_1 , and β are coefficients for describing gas rarefaction impact, which are assigned as 1.19, 4, and 0.4, respectively.

In order to facilitate the evaluation of transport capacity, the conductance, the ratio of gas mass flux to pressure difference, is provided. Notably, in Equation (14), the shrinkage of effective pore size, induced by the adsorption phase thickness, is considered in r_{eff} , and also variation of gas viscosity and Knudsen number manifest the wettability impact.

$$C_{bulk} = \frac{r_{eff}^2 PM}{8\mu RT} (1 + \alpha Kn) \left(1 + \frac{4Kn}{1 - bKn} \right). \quad (14)$$

Meanwhile, real gas effect, denoting that inherent methane molecular volume cannot be overlooked, is coupled in Equation (8). Then, the developed Equation (14) represents the bulk-gas transport conductance in a nanopore. In order to extend its applicability, further work can be devoted to upscaling the pore-scale investigation to nanoscale porous media.

3.4. Surface Diffusion Behavior. Different from the bulk-gas transport behavior, driven by displacement pressure, the mobility of the adsorption molecule is governed by surface diffusion, driven by molecular concentration gradient. At the equilibrium state, the adsorption molecules hop from the adsorption region to the bulk-like region, and the exchange velocity is the same. In the case of a nanopore with a displacement pressure, indicating that the pressure at the inlet is higher than that at the exit, the molecular concentration at the inlet is greater than that at the exit. For the adsorption phase, the concentration gradient takes place, resulting in the adsorption molecules moving from the inlet to the exit. The above physical process is the surface diffusion, on the basis of the analysis, which is closely related to pressure and surface coverage, a key factor representing the ratio of realistic adsorption amount to the maximum value. Wu et al. have established a model for surface diffusion [77], correlating the diffusion capacity with pressure difference, neglecting the capillary pressure between the vapor phase and adsorption phase.

$$J_{surf} = D_s \frac{C_{sc}}{P} \frac{dP}{dl}, \quad (15)$$

where J_{surf} denotes gas mass flux contributed by surface diffusion, kg/m²/s; D_s is the diffusion coefficient, while gas coverage factor is zero, m²/s; and C_{sc} denotes the gas concentration, derived from the single-layer adsorption assumption, kg/m³.

$$C_{sc} = \frac{4\phi M}{\pi\sigma^3 N_A}, \quad (16)$$

TABLE 1: The basic parameters to reproduce the bulk-like gas flow behavior.

Contributors	Method	Material	Pressure	Kn range	Contact angle [#]
Loyalka and Hamoodi [82]	LBM	/	Low pressure	$10^{-3} \sim 10$	30°
Tison [83]	Experiments	Stainless steel tube	0.1 ~ 400 KPa	Entire range	60°

[#]Contact angle information is not available in previous references; its determination relies on the surface material, fluid type, and fitting results comprehensively.

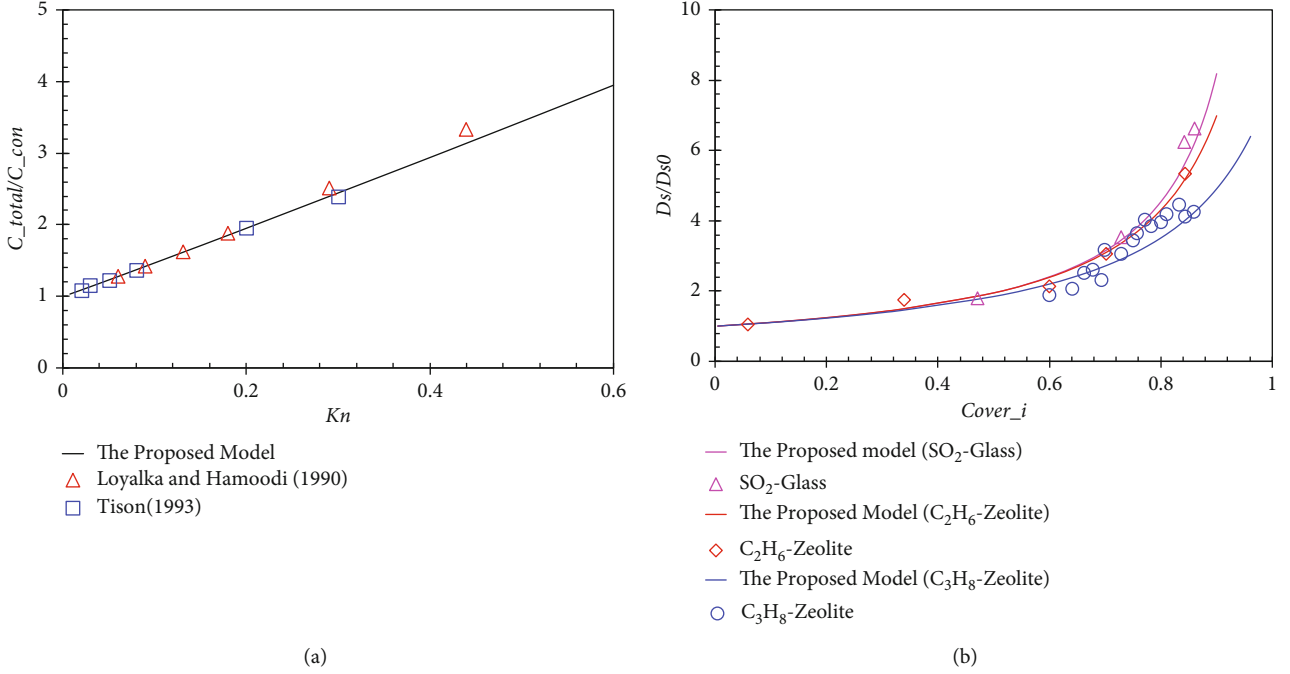


FIGURE 2: The verification of the proposed model: (a) the bulk-gas flow model utilizing the ratio of nanoconfined gas conductance and that for no-slip NS equation; (b) the surface diffusion model utilizing the diffusion coefficient ratio.

$$D_s^o = 8.29 \times 10^{-7} T^{0.5} \exp\left(-\frac{\Delta H^{0.8}}{RT}\right), \quad (17)$$

$$D_s = D_s^o \frac{(1-\phi) + (\kappa/2)\phi(2-\phi) + \{H(1-\kappa)\}(1-\kappa)(\kappa/2)\phi^2}{(1-\phi + (\kappa/2)\phi)^2}, \quad (18)$$

$$H(1-\kappa) = 0, \kappa > 1, \quad (19)$$

$$H(1-\kappa) = 1, \kappa \leq 1, \quad (20)$$

$$\kappa = \frac{\kappa_b}{\kappa_m}, \quad (21)$$

where D_s denotes the diffusion coefficient under a specified gas coverage, m^2/s ; Φ denotes the gas coverage factor, dimensionless; κ_m denotes the molecular potential for forward migration, m/s; and κ_b denotes the molecular potential for blockage, m/s. Notably, the κ is assigned as 0.5, and isosteric adsorption heat at zero coverage (ΔH) is 1.6×10^4 J/mol.

The precondition for the above formulas is the single-layer adsorption assumption [78, 79], suggesting that the surface will be fully occupied with the thickness of a molec-

TABLE 2: The basic parameters to reproduce the surface diffusion.

Gas type	Surface	κ	Temperature	Contact angle [#]
SO ₂ [84]	Glass	0	288 K	12°
C ₂ H ₆ [85]	Zeolite	0.2	323 K	15°
C ₃ H ₈ [86]	Zeolite	0.3	323 K	20°

Contact angle information is not available in previous references; its determination relies on the surface material, fluid type, and fitting results comprehensively.

TABLE 3: The basic parameters for nanoconfined gas transport investigation.

Parameter	Symbol	Unit	Value
Gas type	CH ₄	/	/
Molecular weight	M	g/mol	16
Langmuir pressure	P_L	MPa	2
Ratio for surface diffusion	κ	/	0.5
Adsorption heat when Φ is 0	ΔH	J/mol	16000
Pore size	r	nm	2~100
Contact angle	θ	$^\circ$	0~180
Pressure	P	MPa	0.1~50

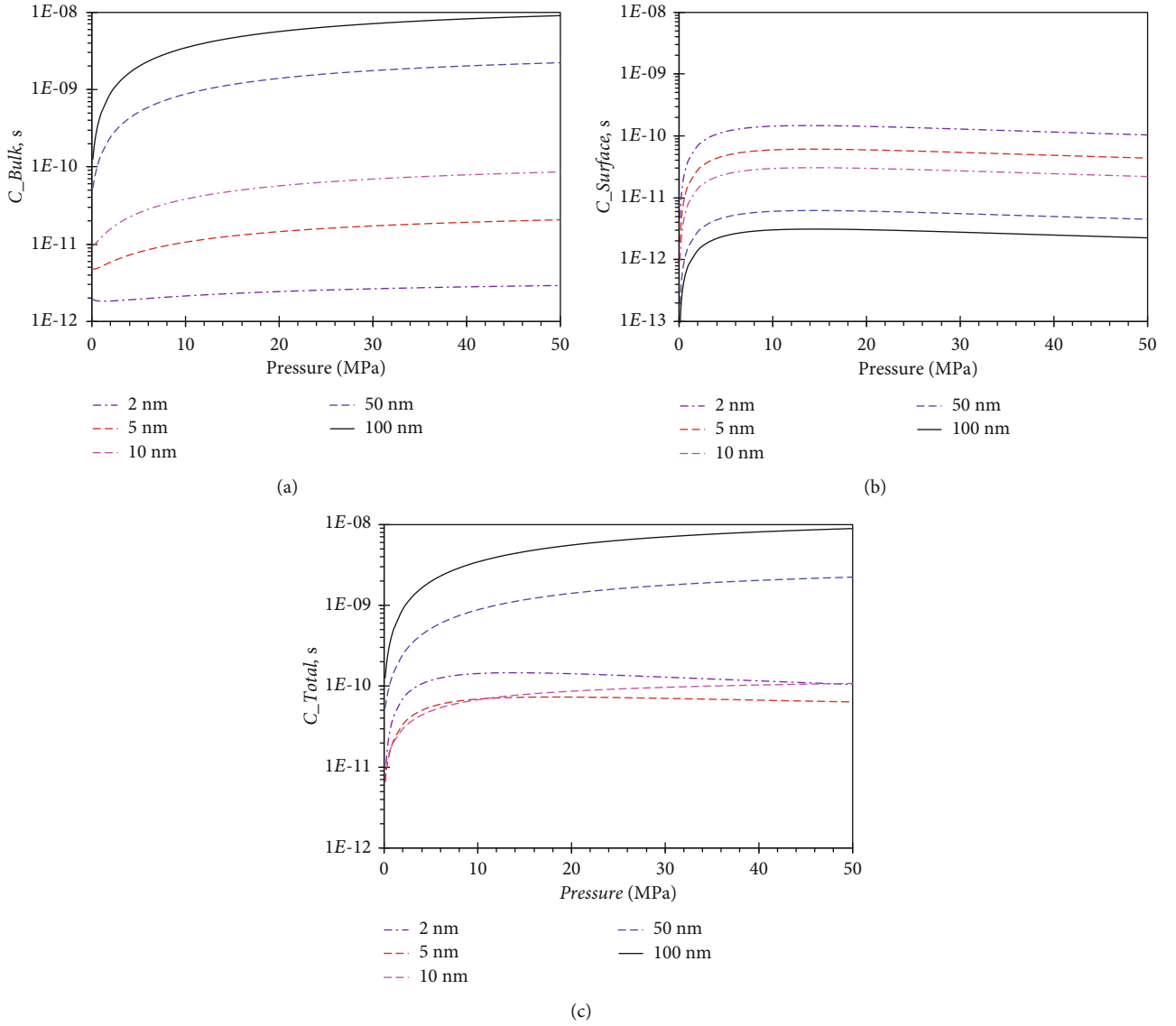


FIGURE 3: Nanoconfined gas flow behavior in the organic nanopore: (a) Bulk-like gas transport behavior; (b) Surface diffusion of adsorption molecules; (c) Total gas conductance.

ular diameter, when the gas coverage approaches 1. Notably, in this article, the adsorption phenomenon is correlated with surface wettability; thus, the gas coverage, with the definition of current adsorption amount to the maximum amount, is related to the surface contact angle. In Section 3.2, focusing on the calculation of adsorption thickness, thickness, obtained from the formula, will always be smaller than a methane molecular diameter; therefore, the single-layer assumption holds during the model establishment. Then, the traditional gas coverage was described as a function of pressure; however, the wettability effect is considered in this article.

$$\phi = \frac{P/Z}{P_L + P/Z} \times \frac{h_{ad}}{\sigma}. \quad (22)$$

Similarly, to facilitate the upcoming comparison, the gas mass flux is transformed as the conductance, which is provided below.

$$C_{surf} = D_s \frac{C_{sc}}{P}. \quad (23)$$

3.5. *Total Nanoconfined Flow in Organic Pores.* Coupling the bulk-like gas conductance and surface diffusion, the total gas flow capacity through an organic nanopore can be evaluated. In this article, an area-average concept is utilized to couple both two flow mechanisms. The concept has been widely applied in the nanoconfined fluid flow theory, like the evaluation of nanoconfined water viscosity and identification of adsorption fluid molecules. Also, some research efforts for nanoconfined gas behavior have achieved good results under the concept. The main

discrepancy between this work and previous contributions is the consideration of wettability impact. As stated and derived in the aforementioned context, the adsorption phase thickness, the gas viscosity, and adsorption coverage are all related to surface contact angle. As a result, the research can be regarded as the previous contributions incorporating surface wettability impact. In sum, the area-average concept is doable to handle this issue.

$$C_{\text{total}} = \left(1 - \frac{h_{ad}}{r}\right)^2 C_{\text{bulk}} + \left(1 - \left(1 - \frac{h_{ad}}{r}\right)^2\right) C_{\text{surf}}, \quad (24)$$

where C_{total} is the gas flow capacity through a specified organic nanopore, s.

The adsorption thickness is a function of pressure and will decline with a decreasing pressure when the other conditions remain unchanged. Thus, the alteration of the weight coefficients for C_{bulk} and C_{surf} happens, demonstrating the nanoconfined flow capacity always change with pressure. This phenomenon highlights the research value for the efficient development of shale gas reservoirs, as the proposed model can capture the change principle of the realistic gas flow capacity under the depressurization process of shale gas reservoirs. Besides, in terms of the realistic development process [80, 81], the pore radius will experience the shrinkage impact, induced by the stress dependence, and the enlarge impact, exerted by the matrix shrinkage. However, in this article, the potential factors, upon original pore size, are not coupled at this point. The proposed model can be further modified by taking care of these factors in the future. This work focuses on the wettability effect on pore-scale gas flow performance.

4. Model Validation

Before the proposed model can be utilized to investigate gas flow in organic nanopores, its reliability requires careful examination. As described in Section 3, the proposed model consists of two components, including the bulk-gas model and a diffusion model for adsorption molecules. Notably, the wettability effect, in the form of surface contact angle, is incorporated in both bulk-gas model, as well as the surface diffusion model. To current knowledge, experimental results are hard to identify whether the mass flux contributions from the bulk gas or adsorption gas and so does the molecular simulation. In this regard, the above two models are verified separately in this article.

As for the proposed bulk-gas model, the enhance factor, describing the enhancement degree of gas flow rate under the nanoconfinement effect, has the definition as the ratio of conductance calculated by the proposed bulk-gas model to that evaluated by no-slip NS equation. In accordance with the definition, the enhance factor can be obtained, which is a function of Knudsen number. Loyalka and Hamoodi [82] and Tison [83] have provided fruitful data for the nanoconfined bulk-gas flow, with the help of advanced numerical method and laboratory exper-

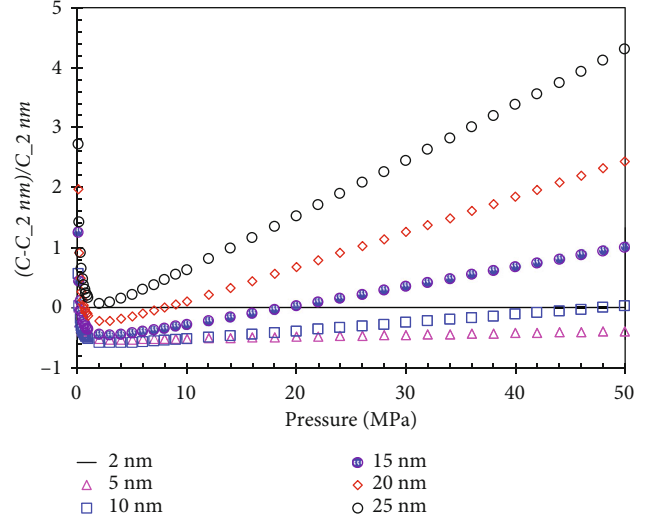


FIGURE 4: Comparison of total gas flux at a specified pore size to that of 2 nm.

iments. Detailed basic data collected from the previous documents is tabulated in Table 1. Notably, in this part, the surface diffusion is neglected, and then the C_{total} is degenerated from Equations (24) to (14). C_{con} denotes the gas conductance based on the no-slip NS equation, and the formula for enhance factor is provided.

$$C_{\text{total}}/C_{\text{con}} = \frac{r_{\text{eff}}^2}{r^2} (1 + \alpha Kn) \left(1 + \frac{4Kn}{1 + Kn}\right). \quad (25)$$

As depicted in Figure 2(a), it can be demonstrated that the proposed bulk-gas model is able to achieve good agreements with existed simulation results and experimental data. Also, based on the relationship between gas conductance and Knudsen number, it can be inferred that the gas rarefaction, induced by the nanoconfinement impact, plays a positive role for gas transport capacity. Concrete underlying mechanisms will be specified in the following discussion part. As for the proposed surface diffusion model, the ratio of diffusion coefficient at a given gas coverage to that at zero gas coverage is used. Similarly, relevant data is collected from the previous references, in which gas type includes SO_2 , C_2H_6 , and C_3H_8 , and detailed information is presented in Table 2.

It can be observed from Figure 2(b) that the proposed model for surface diffusion can reach a good match with the actual recorded value. The surface diffusion becomes evident with the increase of gas coverage, and the enhancement amplitude also climbs with the increasing gas coverage. As the surface diffusion is a unique mechanism for gas-flux contribution, comparing with the gas flow through conventional pores, the nanoconfined gas flow capacity strengthens dramatically. Thus, the difference, between nanoconfined gas behavior and bulk gas, arises in both the bulk-like gas flow and surface diffusion. With the intent of capturing gas flow behavior in the organic nanopore, one should take care

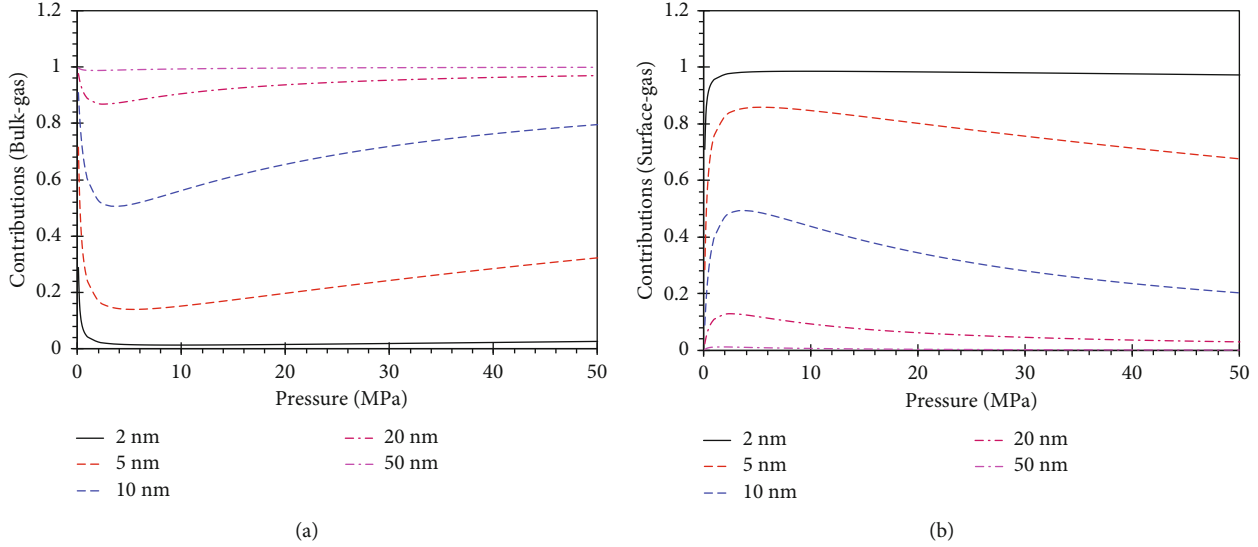


FIGURE 5: Contributions to the total gas conductance: (a) Bulk-like gas; (b) Adsorption gas molecules.

of both the bulk-like gas transport model and surface diffusion model.

5. Results and Discussion

After clarifying the reliability of the proposed model, it is sensible to shed light on gas flow behavior in the organic nanopore, with the help of the above research efforts. Actually, previous contributions have been performed to investigate the issue; however the wettability effect, denoting the surface affinity to methane molecules and becoming more evident in a nanoscale space, has received little attention. In this article, we focus on the wettability effect on the gas flow behavior, looking forward to enriching relevant knowledge about shale gas flow mechanisms. Some basic parameters are provided in Table 3, facilitating the analysis upon influential factors.

5.1. Nanoconfined Flow Conductivity. To date, the discrepancy between the nanoconfined gas flow behavior and that in bulk state has been widely reported. Intuitively, the discrepancy stems from the shrinkage of pore scale, suggesting the pore size influence. A general knowledge in terms of the role of pore size is urgent. Five sets of pore size are utilized here, including 2 nm, 5 nm, 10 nm, 50 nm, and 100 nm, covering the entire pore size range of the organic shale nanopores. And, in this part, the surface contact angle remains unchanged as 30° , and the other parameters are used from Table 3. As depicted in Figure 3, the nanoconfined gas flow behavior over the pressure, ranging from 0.1 to 50 MPa, is presented. In the case of bulk-like gas, the conductance increases with the increasing pressure. The greater methane density, under the higher pressure, is supposed to take responsible for this phenomenon. Also, the high-pressure atmosphere will mitigate the methane free path, resulting in small Knudsen number; therefore, the molecules at boundary may lose mobility. As a result, the high-pressure

atmosphere can impair the gas conductance, regardless of the enhance effect based on the methane density. Meanwhile, at a specific pressure, bulk-gas conductance has a positive correlation with pore size. However, the gas conductance, contributed by surface diffusion, has a negative correlation with pore size. It is because the volume-weight coefficient for adsorption gas becomes greater with the decline of pore size. For example, as the adsorption phase thickness falls in a small range, as inferred from Equation (5), the volume-weight coefficient for surface diffusion in 2 nm will far beyond that in 100 nm. In addition, from Figure 3(b), for a specific pore size, the conductance will increase rapidly at first and then become stable with the increasing pressure. The first stage for rapid increase is mainly attributed by the dramatical increase of diffusion coefficient (D_s) as well as gas concentration (C_{sc}), and both are sensitive to the variation of pressure.

After analyzing the flow behavior of bulk-like gas and adsorption molecules separately, the total gas conductance, directly manifesting the gas flow capacity in the organic nanopore, is presented in Figure 3(c). It can be observed that the pore size has little impact on the general variation feature between the gas conductance and pressure; gas flow capacity always has a positive relationship with increasing pressure. In order to achieve a clear image about total gas conductance, for the pressure ranging from 0.1 to 50 MPa, it is surprising to find that total conductance in 5 nm and 10 nm is less than that in 2 nm. Also, in Figure 4, the total gas conductance in 15 nm and 20 nm is less than 2 nm in the pressure range of 0.1~20 nm and 0.1~8 MPa, respectively. Based on the traditional theory, the greater pore size corresponds to the stronger gas flow capacity, while the nanoconfined gas flow behavior can alter the above perspective. The phenomenon can be attributed to the role of surface diffusion, which is dominant in nanopores with pore size less than 5 nm. It should be noted that the traditional theory roots in the bulk-gas flow mechanism and overlooks the surface

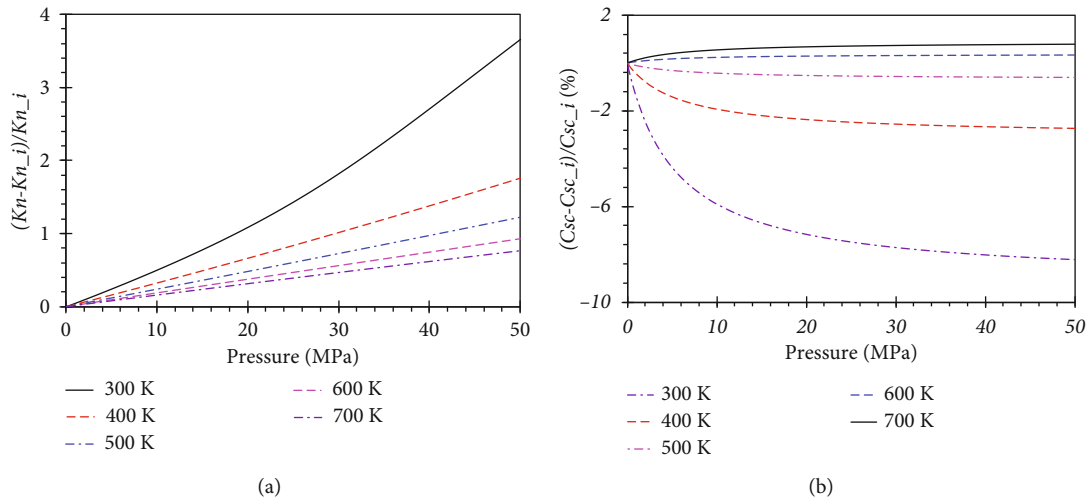


FIGURE 6: Variation of key parameters caused by real gas effect: (a) Kn ; (b) Gas concentration.

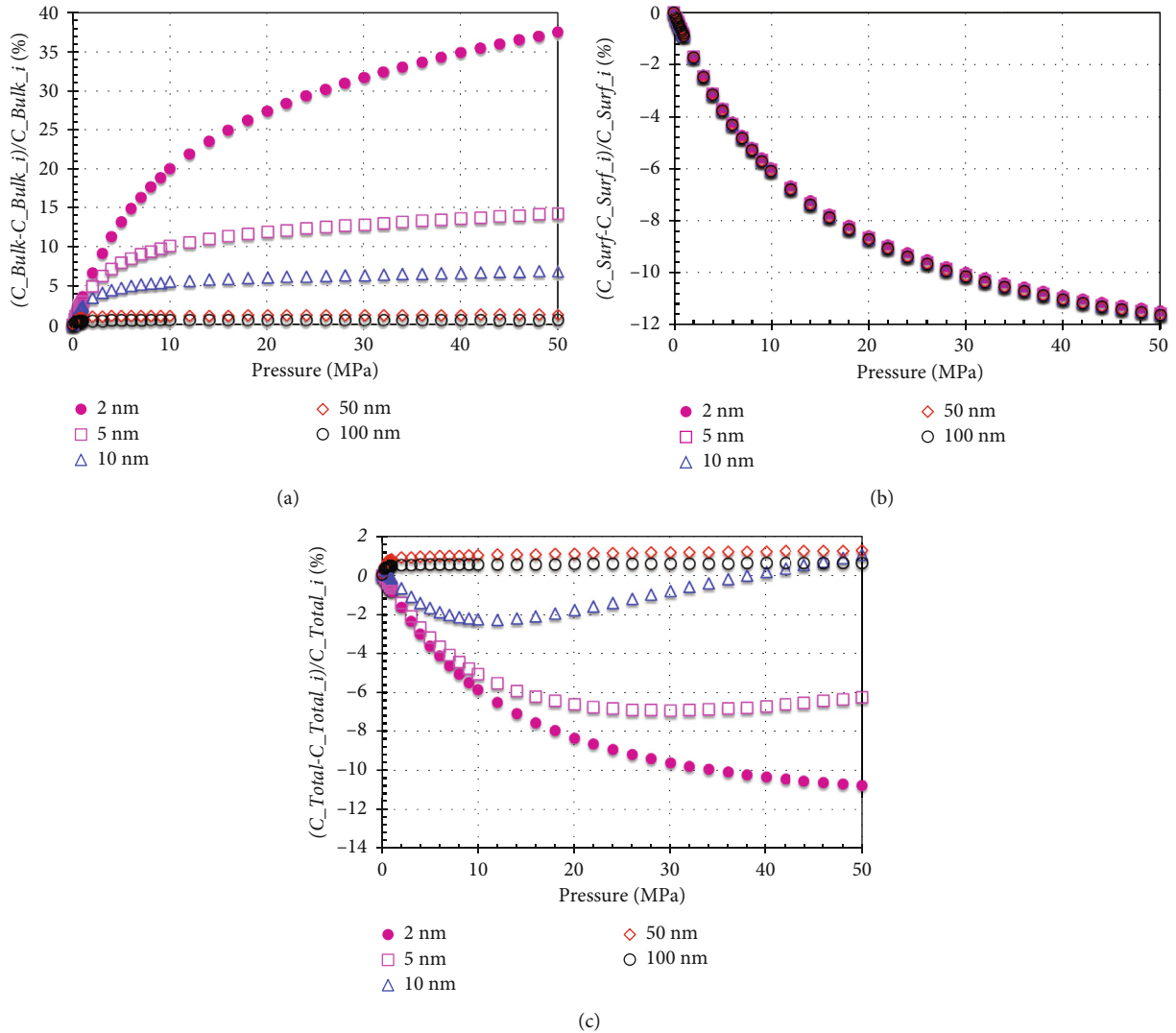


FIGURE 7: Deviation caused by the real gas effect: (a) Bulk-like gas conductance; (b) Surface diffusion; (c) Total gas conductance.

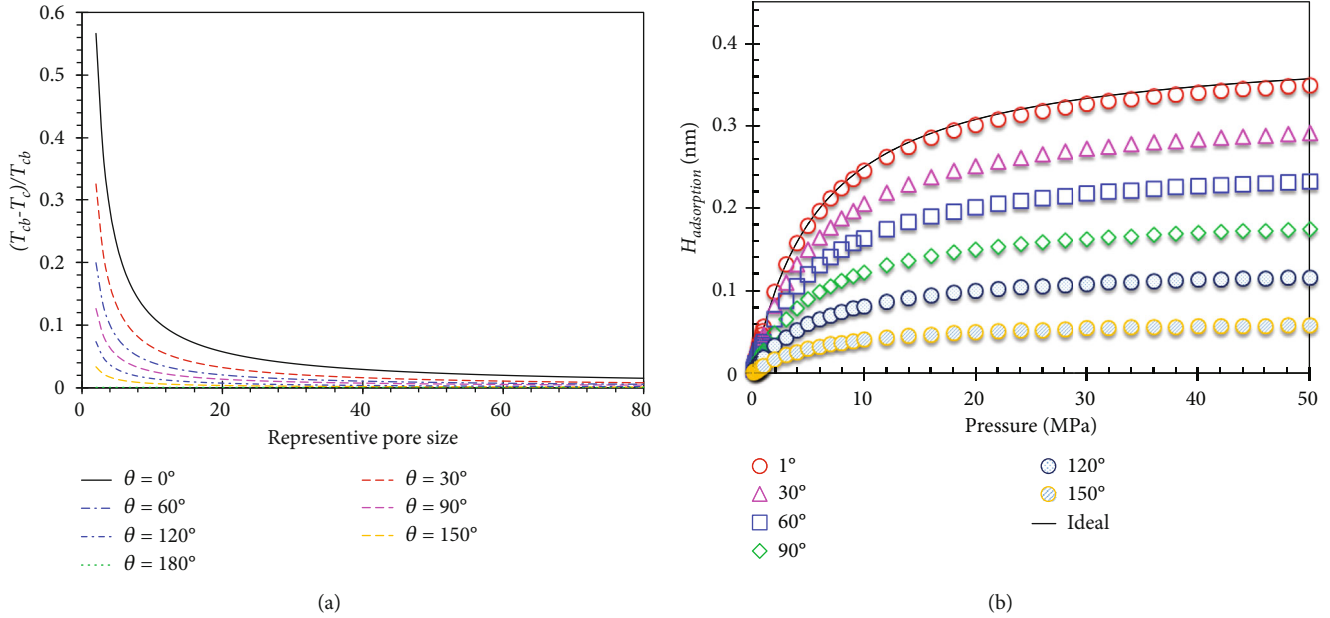


FIGURE 8: The variation of key parameters caused by wettability impact: (a) Critical properties; (b) Adsorption phase thickness.

diffusion. Thus, although the gas conductance in small pores, contributed by bulk gas, is less than that in large pores, the gas conductance, contributed by surface diffusion, may drastically enhance gas flow capacity and allow gas conductance in small pores greater than that in the large pores. The observation is helpful to understand shale gas production behavior in field.

The contributions of bulk-like gas and adsorption molecules are presented in Figure 5. It can be concluded that surface diffusion is dominant for pore size less than 5 nm and bulk-gas flow mechanism becomes the prominent contributor for pore size larger than 50 nm. When pore size falls in the range of 5~50 nm, the relative strengths of bulk-gas flow mechanism and surface diffusion are heavily dependent on pressure. The contribution of bulk-gas conductance will decrease first and then increase stable. On the contrary, the contribution of surface diffusion will increase first and then decrease stable. It is the variation feature that the gas conductance in small pores can exceed that in large pores. Thus, the gas flow capacity through nanopores may be underestimated based on the current theory, and the surface diffusion contribution cannot be neglected for small nanopores.

5.2. Real Gas Effect. In realistic shale organic nanopores, the atmosphere pressure can reach as high as 50 MPa. And, the gas molecules cannot be considered as ideal gas under this condition, as frequency of intermolecular collision climbs a lot, and intermolecular distance becomes comparable to molecular diameter. Associated influence will arise by considering the molecular inherent diameter, such as the variation of gas viscosity and compressibility, as well as MFP, which is called as real gas effect. For previous pieces of research efforts in biological or physical scope, due to the small atmosphere pressure, gas molecules are widely regarded as the real gas effect. However, the assumption

appears to break down for shale gas reservoirs. Notably, for ideal gas, the gas viscosity (μ) remains unchanged as the gas viscosity at the standard condition (μ_{atm}), regardless of alteration of pressure and temperature. And the idea gas compressibility (Z) is always 1. In the following comparison, the original symbol with an additional i suggests the physical parameter for ideal gas assumptions. The other parameters are used from Table 3.

Similar to the verification section, the bulk-gas flow mechanism and surface diffusion are investigated separately. In Figure 6(a), the Knudsen number for real gas can reach as great as 3 times that of ideal gas. Also, the magnitude increases with the increasing pressure. Notably, the discrepancy, induced by real gas effect, upon Knudsen number disappears, while the pressure approaches 0.1 MPa. This phenomenon meets the above analysis that the real gas behavior can be regarded as the same as ideal gas under low pressure. Therefore, the bulk-gas flow capacity will be underestimated, while the real gas effect is not considered. At a specified pressure, the real gas effect will be mitigated by enhancing temperature. As for the surface diffusion, the gas concentration is utilized to shed light on the real gas effect. In the case of temperature less than 500 K in Figure 6(b), the gas concentration will decline with the increasing pressure, and the magnitude can reach as great as 8%. In contrast, when temperature exceeds 500 K, the gas concentration will show a slightly increase trend. The above phenomenon is mainly caused by the dependency of natural gas compressibility on surrounding temperature.

With the intent of quantifying the real gas effect, the concrete deviation is calculated and presented in Figure 7. As depicted in Figure 7(a), due to the existence of real gas effect, gas conductance will be enhanced, and the magnitude can reach 15% when pore size is equal to 5 nm. Notably, the magnitude will be greatly mitigated in large nanopores, and

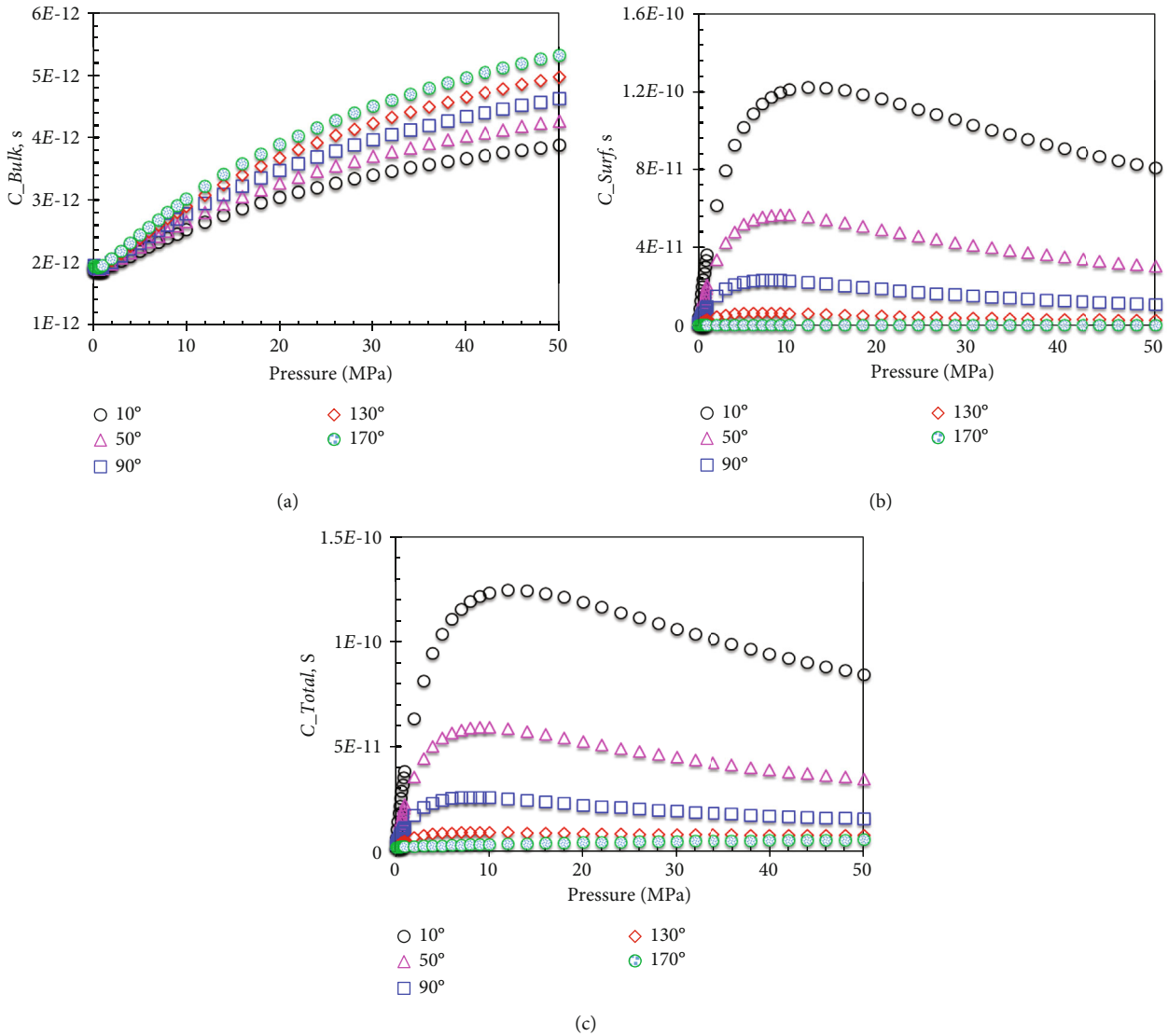


FIGURE 9: Wettability impact on gas transport through organic nanopore when pore size is equal to 2 nm: (a) Bulk-like gas conductance; (b) Surface diffusion; (c) Total gas conductance.

it will be close to zero for pore size beyond 50 nm. As for surface diffusion in Figure 7(b), the gas conductance shows a negative relationship with regard to pressure, indicating that real gas effect indeed impairs the contributions from surface diffusion. The relationship is insensitive to the variation of pore size. In Figure 7(c), combining the bulk-like gas flow mechanism and surface diffusion, the negative correlation between pressure and total gas conductance holds when pore size is less than 10 nm. However, when pore size exceeds 50 nm, the gas conductance will increase with increasing pressure. The relative contribution of gas flow mechanisms, presented in Figure 5, can be used to elucidate the issue. For small nanopores, the prominent factor, in terms of the total gas conductance, is surface diffusion and turns to be bulk-like gas flow for large nanopores. As a result, the total conductance will show the negative correlation with increasing pressure, keeping in line with the surface diffusion, and show the positive correlation, keeping in line with the bulk-like gas conductance.

5.3. Wettability Effect. In shale, the surface affinity for organic nanopores is diversity, relying on the surface composition and pore size, as well as physical structure. Also, shale is a highly-developed heterogeneous porous media across thousands of geological years [87, 88]. There exists a variety of kerogen molecular types, known as the basic components for shale organic nanopores, as well as a wide range of thermal maturity, which will result in different surface wettability upon shale gas. Also, considering the mineral composition in the organic nanopores, particularly at the low-maturity period, the surface contact angle is set to fall in the range of 0~180°. The other parameters are used in Table 3.

In this article, the wettability effect is represented by the methane critical properties and adsorption phase thickness, both which are heavily dependent on the surface contact angle. As depicted in Figure 8(a), the critical temperature will decline with the pore size shrinkage. Also, at a specified pore size, strong surface affinity corresponds to the large

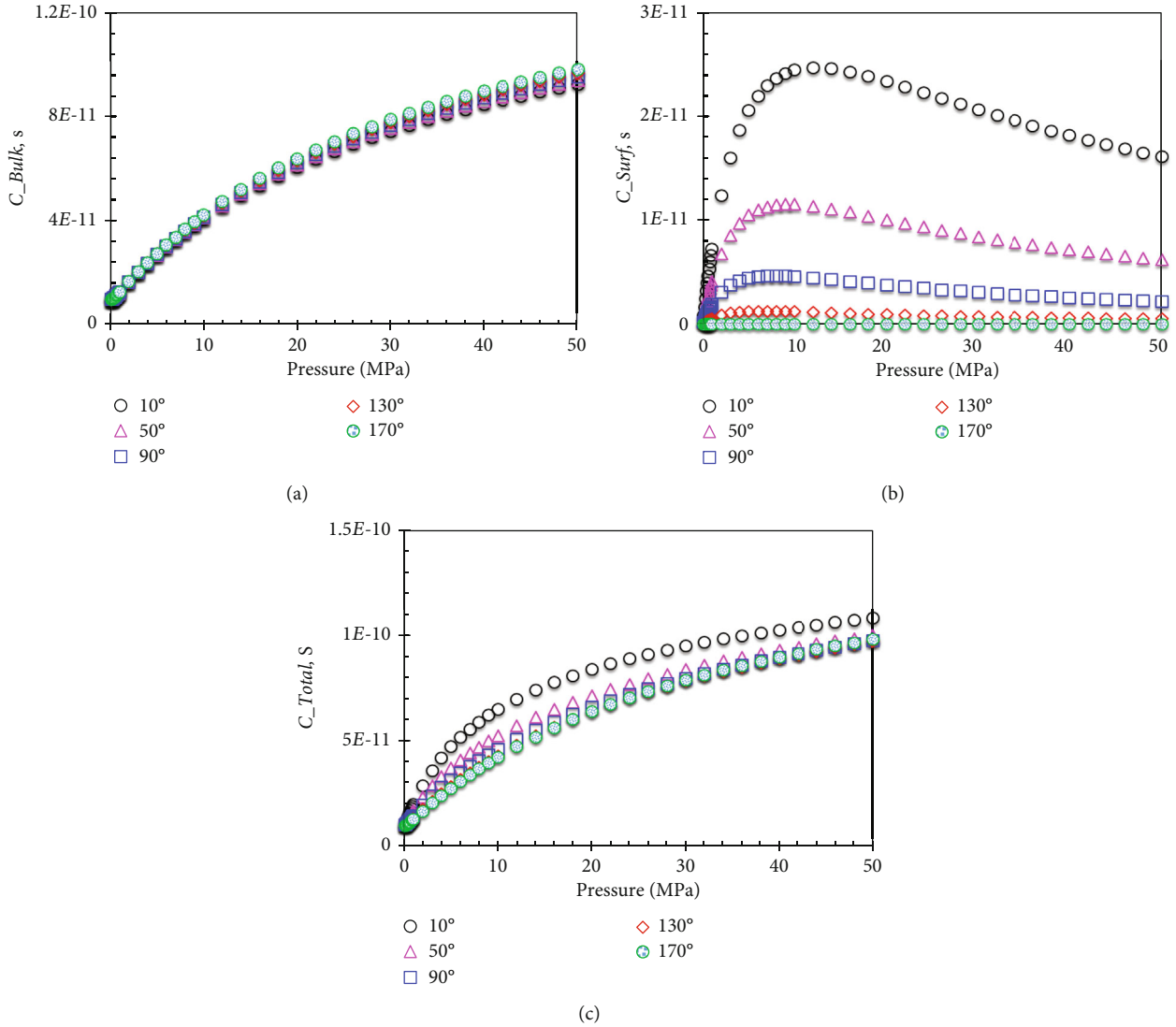


FIGURE 10: Wettability impact on gas transport through organic nanopore when pore size is equal to 10 nm: (a) Bulk-like gas conductance; (b) Surface diffusion; (c) Total gas conductance.

decreasing magnitude, manifesting the influence of strong interactions between surface and molecules. In Figure 8(b), the adsorption phase thickness versus surface contact angle is presented. As for the strong surface affinity, the adsorption thickness will approach the ideal gas. And the adsorption phenomenon will disappear for extreme weak surface affinity, imposing a repulsive force upon the methane molecules near the surface.

As for small nanopores with pore size of 2 nm, the wettability effect on gas conductance, contributed by bulk-like gas and adsorption gas, is quantified. In Figure 9(a), it can be found that bulk-gas conductance will decrease while the surface affinity strengthens. Similarly, Figure 9(b) denotes the variation feature of surface diffusion versus pressure, indicating that the gas conductance, contributed by surface diffusion, will enhance with strong surface affinity. After comparison, it can be concluded that the deviation of bulk-gas conductance caused by surface wettability is smaller than the surface diffusion. Hence, wettability impact has minor

influence on the bulk-gas flow mechanism and major influence on the surface diffusion. Furthermore, on the basis of Figure 9(c), the tendency of total gas conductance versus pressure is close to that for surface diffusion, which is caused by the dominant role of surface diffusion in small nanopores.

When pore size becomes 10 nm, the overall impact, induced by surface wettability, on gas conductance changes. In Figure 10(a), the tendency is the same with that in Figure 9(a); however, the discrepancy caused by the surface wettability becomes smaller, comparing with that in 2 nm. It demonstrates that the wettability impact on bulk-gas flow behavior will become weak with the increasing pore size. Additionally, wettability effect on surface diffusion remains unchanged, comparing with that in 2 nm, as presented in Figure 10(b). In the meanwhile, the total conductance versus pressure shows dramatic difference with that in 2 nm, which can be explained by the relative contributions, presented in Figure 5. The wettability impact has little influence on

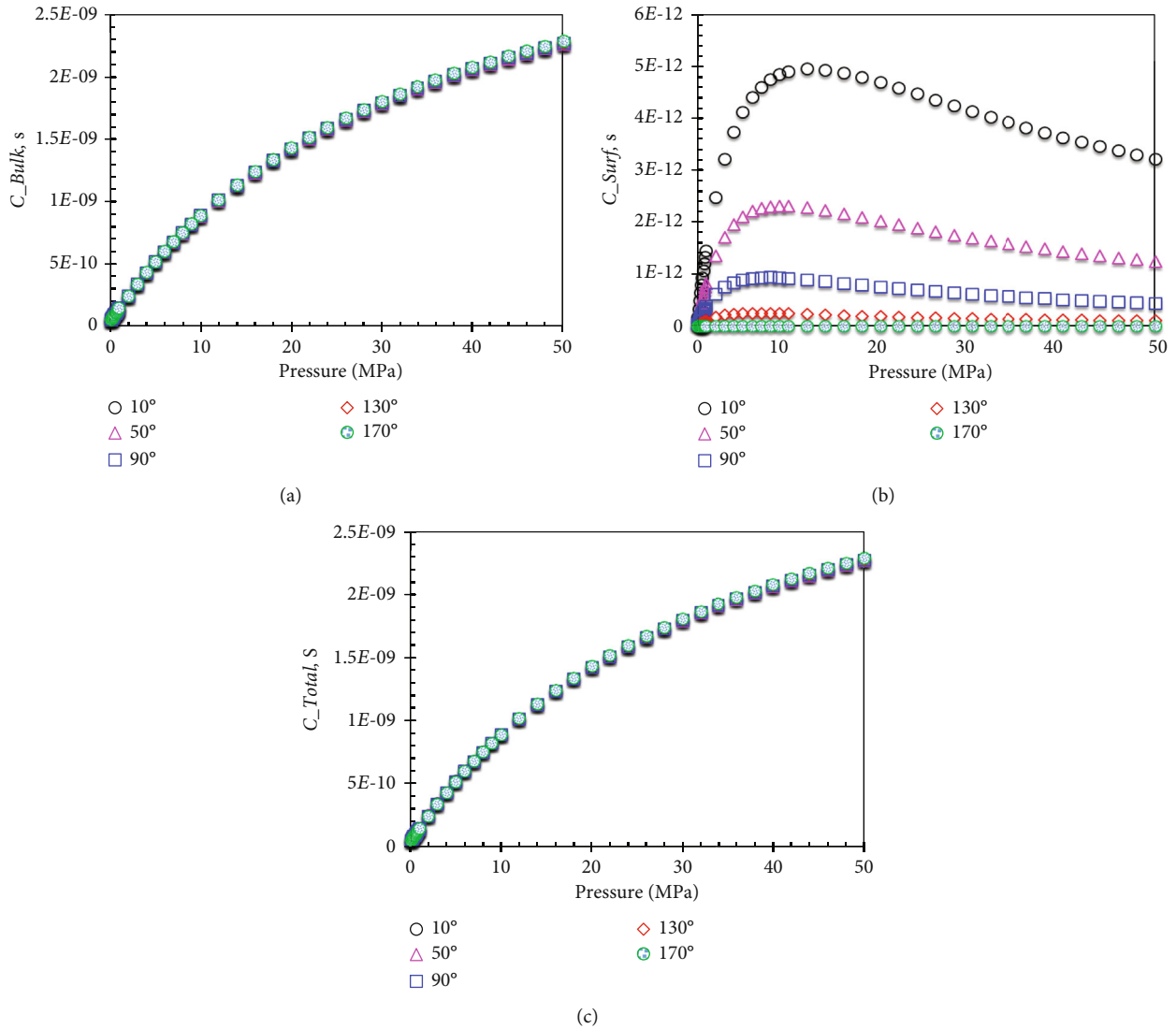


FIGURE 11: Wettability impact on gas transport through organic nanopore when pore size is equal to 50 nm: (a) Bulk-like gas conductance; (b) Surface diffusion; (c) Total gas conductance.

bulk-gas flow behavior in large nanopores, and mainly affects the surface diffusion. Thus, the total gas conductance versus pressure will approach that for surface diffusion in 2 nm and approach the bulk-like gas flow mechanism when pore size is beyond 10 nm.

Regularity of nanoconfined flow behavior in the organic nanopore with pore size of 50 nm is presented in Figure 11, demonstrating the correctness of the aforementioned analysis. In the large nanopore, the total conductance and bulk-like gas conductance share the same variation feature, regardless of the wettability effect on surface diffusion. As a result, in the case of the total gas flow capacity, the wettability effect has little impact when pore size is beyond 50 nm, while it cannot be neglected when pore size is less than 10 nm. Accordingly, the wettability impact has the applicability scope, suggesting the upper limit of pore size is 10 nm, which is in line with the surface diffusion. In light of the fact that massive shale organic nanopores have pore

size less than 10 nm, thus the wettability impact is worthy of consideration for precise flow behavior characterization.

6. Conclusions

- (1) A robust model for gas flow through the shale organic nanopore is developed, coupling surface wettability into both bulk-gas flow model, as well as surface diffusion model. Key factors, induced by surface wettability and pore size shrinkage, are considered properly, including the critical property shift, gas viscosity variation, and adsorption phase thickness
- (2) Gas conductance, contributed by bulk-gas flow mechanism, has a positive relationship with pore size; however that from surface diffusion has the opposite trend. The gas flux in small nanopores may exceed that in large nanopores, due to the predominant role of

surface diffusion while pore size is less than 10 nm. Absence of real gas effect will lead to inaccurate characterization of nanoconfined gas flow capacity, the magnitude can reach 7% for pore size of 5 nm

- (3) The wettability impact has little influence on bulk-gas flow behavior and mainly affects the surface diffusion. Wettability effect governs the total gas flux when pore size is less than 10 nm, while its impact will be greatly mitigated when pore size is greater than 50 nm. The wettability impact has the applicability scope, and its upper limit of pore size is 10 nm

Data Availability

Data is available on request.

Conflicts of Interest

The authors declare that they have no conflicts of interest.

Acknowledgments

We acknowledge China University of Mining & Technology for the permission to publish this work.

References

- [1] P. Mastropietro, P. Rodilla, and C. Batlle, "Emergency measures to protect energy consumers during the Covid-19 pandemic: a global review and critical analysis," *Energy Research & Social Science*, vol. 68, p. 101678, 2020.
- [2] J. Millward-Hopkins, J. K. Steinberger, N. D. Rao, and Y. Oswald, "Providing decent living with minimum energy: a global scenario," *Global Environmental Change*, vol. 65, p. 102168, 2020.
- [3] Z. Sun, B. Huang, K. Wu et al., "Nanoconfined methane density over pressure and temperature: wettability effect," *Journal of Natural Gas Science and Engineering*, vol. 99, p. 104426, 2022.
- [4] T. Wang, S. Tian, G. Li, L. Zhang, M. Sheng, and W. Ren, "Molecular simulation of gas adsorption in shale nanopores: a critical review," *Renewable and Sustainable Energy Reviews*, vol. 149, p. 111391, 2021.
- [5] V. Ş. Ediger, J. V. Bowlus, and A. F. Dursun, "State capitalism and hydrocarbon security in China and Russia," *Energy Strategy Reviews*, vol. 38, p. 100725, 2021.
- [6] T. Fang, Y. Zhang, B. Ding, Y. Yan, and J. Zhang, "Static and dynamic behavior of CO₂ enhanced oil recovery in nanoslits: effects of mineral type and oil components," *International Journal of Heat and Mass Transfer*, vol. 153, p. 119583, 2020.
- [7] Y. Pang, X. Hu, S. Wang, S. Chen, M. Y. Soliman, and H. Deng, "Characterization of adsorption isotherm and density profile in cylindrical nanopores: modeling and measurement," *Chemical Engineering Journal*, vol. 396, p. 125212, 2020.
- [8] J. Xu, K. Wu, S. Yang et al., "Real gas transport in tapered non-circular nanopores of shale rocks," *AIChE Journal*, vol. 63, no. 7, pp. 3224–3242, 2017.
- [9] H. Song, M. Yu, W. Zhu et al., "Numerical investigation of gas flow rate in shale gas reservoirs with nanoporous media," *International Journal of Heat and Mass Transfer*, vol. 80, pp. 626–635, 2015.
- [10] Q. Zhang, Y. Su, W. Wang, M. Lu, and G. Sheng, "Gas transport behaviors in shale nanopores based on multiple mechanisms and macroscale modeling," *International Journal of Heat and Mass Transfer*, vol. 125, pp. 845–857, 2018.
- [11] Y. Yin, Z. G. Qu, and J. F. Zhang, "Multiple diffusion mechanisms of shale gas in nanoporous organic matter predicted by the local diffusivity lattice Boltzmann model," *International Journal of Heat and Mass Transfer*, vol. 143, p. 118571, 2019.
- [12] P. Yu, D. Dempsey, and R. Archer, "A three-dimensional coupled thermo-hydro-mechanical numerical model with partially bridging multi-stage contact fractures in horizontal-well enhanced geothermal system," *International Journal of Rock Mechanics and Mining Sciences*, vol. 143, p. 104787, 2021.
- [13] Z. Sun, B. Huang, Y. Liu et al., "Gas-phase production equation for CBM reservoirs: interaction between hydraulic fracturing and coal orthotropic feature," *Journal of Petroleum Science and Engineering*, vol. 213, p. 110428, 2022.
- [14] Y. Miao, X. Li, Y. Zhou et al., "A new rate-transient analysis model for shale gas reservoirs coupled the effect of slip flow and surface diffusion," *International Journal of Heat and Mass Transfer*, vol. 124, pp. 1–10, 2018.
- [15] J. Zhao, D. Fu, Y. Li, Y. Jiang, W. Xu, and X. Chen, "REV-scale simulation of gas transport in shale matrix with lattice Boltzmann method," *Journal of Natural Gas Science and Engineering*, vol. 57, pp. 224–237, 2018.
- [16] H. Wang, L. Chen, Z. Qu et al., "Modeling of multi-scale transport phenomena in shale gas production – a critical review," *Applied Energy*, vol. 262, p. 114575, 2020.
- [17] H. Gao, J. Wang, X. Chen et al., "Nanoconfinement effects on thermal properties of nanoporous shape-stabilized composite PCMs: a review," *Nano Energy*, vol. 53, pp. 769–797, 2018.
- [18] A. Fatah, Z. Bennour, H. B. Mahmud, R. Gholami, and M. Hossain, "Surface wettability alteration of shales exposed to CO₂: implication for long-term integrity of geological storage sites," *International Journal of Greenhouse Gas Control*, vol. 110, p. 103426, 2021.
- [19] I. W. R. Saputra, O. Adebisi, E. B. Ladan, A. Bagareddy, A. Sarmah, and D. S. Schechter, "The influence of oil composition, rock mineralogy, aging time, and brine pre-soak on shale wettability," *ACS Omega*, vol. 7, no. 1, pp. 85–100, 2021.
- [20] M. R. Yassin, H. Dehghanpour, J. Wood, and Q. Lan, "A theory for relative permeability of unconventional rocks with dual-wettability pore network," *SPE Journal*, vol. 21, no. 6, pp. 1970–1980, 2016.
- [21] B. Ghanbarian, F. Liang, and H. H. Liu, "Modeling gas relative permeability in shales and tight porous rocks," *Fuel*, vol. 272, p. 117686, 2020.
- [22] Z. Sun, S. Wang, H. Xiong, K. Wu, and J. Shi, "Optimal nanocone geometry for water flow," *AIChE Journal*, vol. 68, no. 3, p. e17543, 2022.
- [23] K. Wang, K. Ye, B. Jiang, H. Li, and Y. Tan, "The mechanism of gas-water extraction in micro- and nanoscale pores in shale gas reservoirs: based on gas-water interactions," *Chemical Engineering Science*, vol. 248, p. 117259, 2022.
- [24] J. Li, X. Li, X. Wang et al., "Water distribution characteristic and effect on methane adsorption capacity in shale clay," *International Journal of Coal Geology*, vol. 159, pp. 135–154, 2016.
- [25] C. R. Clarkson, N. Solano, R. M. Bustin et al., "Pore structure characterization of North American shale gas reservoirs using

- USANS/SANS, gas adsorption, and mercury intrusion,” *Fuel*, vol. 103, pp. 606–616, 2013.
- [26] D. R. Sandoval, W. Yan, M. L. Michelsen, and E. H. Stenby, “Modeling of shale gas adsorption and its influence on phase equilibrium,” *Industrial & Engineering Chemistry Research*, vol. 57, no. 17, pp. 5736–5747, 2018.
- [27] Z. Sun, B. Huang, Y. Li, H. Lin, S. Shi, and W. Yu, “Nanoconfined methane flow behavior through realistic organic shale matrix under displacement pressure: a molecular simulation investigation,” *Journal of Petroleum Exploration and Production Technology*, vol. 12, no. 4, pp. 1193–1201, 2022.
- [28] L. Huang, W. Zhou, H. Xu, L. Wang, J. Zou, and Q. Zhou, “Dynamic fluid states in organic-inorganic nanocomposite: implications for shale gas recovery and CO₂ sequestration,” *Chemical Engineering Journal*, vol. 411, p. 128423, 2021.
- [29] S. Jribi, T. Miyazaki, B. B. Saha et al., “Equilibrium and kinetics of CO₂ adsorption onto activated carbon,” *International Journal of Heat and Mass Transfer*, vol. 108, pp. 1941–1946, 2017.
- [30] E. Fathi and I. Y. Akkutlu, “Multi-component gas transport and adsorption effects during CO₂ injection and enhanced shale gas recovery,” *International Journal of Coal Geology*, vol. 123, pp. 52–61, 2014.
- [31] K. Wu, Z. Chen, X. Li et al., “Flow behavior of gas confined in nanoporous shale at high pressure: real gas effect,” *Fuel*, vol. 205, pp. 173–183, 2017.
- [32] S. Yang, K. Wu, J. Xu, J. Li, and Z. Chen, “Roles of multicomponent adsorption and geomechanics in the development of an Eagle Ford shale condensate reservoir,” *Fuel*, vol. 242, pp. 710–718, 2019.
- [33] R. Li, Z. Chen, K. Wu, X. Hao, and J. Xu, “An analytical model for water-oil two-phase flow in inorganic nanopores in shale oil reservoirs,” *Petroleum Science*, vol. 18, no. 6, pp. 1776–1787, 2021.
- [34] X. Wang, J. Chen, D. Ren, and Z. Shi, “Role of gas viscosity for shale gas percolation,” *Geofluids*, vol. 2020, 10 pages, 2020.
- [35] M. Dejam, “Advective-diffusive-reactive solute transport due to non-Newtonian fluid flows in a fracture surrounded by a tight porous medium,” *International Journal of Heat and Mass Transfer*, vol. 128, pp. 1307–1321, 2019.
- [36] M. Dejam, H. Hassanzadeh, and Z. Chen, “Semi-analytical solution for pressure transient analysis of a hydraulically fractured vertical well in a bounded dual-porosity reservoir,” *Journal of Hydrology*, vol. 565, pp. 289–301, 2018.
- [37] S. Wang, Q. Feng, F. Javadpour, M. Zha, and R. Cui, “Multi-scale modeling of gas transport in shale matrix: an integrated study of molecular dynamics and rigid-pore-network model,” *SPE Journal*, vol. 25, no. 3, pp. 1416–1442, 2020.
- [38] H. Wang, Z. Qu, Y. Yin, J. Bai, and B. Yu, “Review of molecular simulation method for gas adsorption/desorption and diffusion in shale matrix,” *Journal of Thermal Science*, vol. 28, no. 1, pp. 1–16, 2019.
- [39] L. Zhang, C. Liu, Q. Li, S. Wang, S. Cai, and E. Huo, “Shale gas transport through the inorganic cylindrical and conical nanopores: a density gradient driven molecular dynamics,” *International Journal of Heat and Mass Transfer*, vol. 183, p. 122126, 2022.
- [40] Z. Sun, X. Li, W. Liu, T. Zhang, M. He, and H. Nasrabadi, “Molecular dynamics of methane flow behavior through realistic organic nanopores under geologic shale condition: pore size and kerogen types,” *Chemical Engineering Journal*, vol. 398, p. 124341, 2020.
- [41] Z. Sun, B. Huang, S. Yan et al., “Nanoconfined methane thermodynamic behavior below critical temperature: liquid–vapor coexistence curve under wettability effect,” *Industrial & Engineering Chemistry Research*, vol. 61, no. 14, pp. 4971–4979, 2022.
- [42] H. Yu, J. Fan, J. Xia, H. Liu, and H. Wu, “Multiscale gas transport behavior in heterogeneous shale matrix consisting of organic and inorganic nanopores,” *Journal of Natural Gas Science and Engineering*, vol. 75, p. 103139, 2020.
- [43] H. Yu, H. Xu, J. Fan, F. Wang, and H. Wu, “Roughness factor-dependent transport characteristic of shale gas through amorphous kerogen nanopores,” *The Journal of Physical Chemistry C*, vol. 124, no. 23, pp. 12752–12765, 2020.
- [44] T. Zhang, X. Li, X. Wang et al., “Modelling the water transport behavior in organic-rich nanoporous shale with generalized lattice Boltzmann method,” *International Journal of Heat and Mass Transfer*, vol. 127, pp. 123–134, 2018.
- [45] J. Huang, F. Xiao, C. Labra, J. Sun, and X. Yin, “DEM-LBM simulation of stress-dependent absolute and relative permeabilities in porous media,” *Chemical Engineering Science*, vol. 239, p. 116633, 2021.
- [46] M. Sheikholeslami, “Influence of magnetic field on Al₂O₃-H₂O nanofluid forced convection heat transfer in a porous lid driven cavity with hot sphere obstacle by means of LBM,” *Journal of Molecular Liquids*, vol. 263, pp. 472–488, 2018.
- [47] J. Zhao, J. Yao, L. Zhang, H. Sui, and M. Zhang, “Pore-scale simulation of shale gas production considering the adsorption effect,” *International Journal of Heat and Mass Transfer*, vol. 103, pp. 1098–1107, 2016.
- [48] J. Huang, X. Yin, M. Barrufet, and J. Killough, “Lattice Boltzmann simulation of phase equilibrium of methane in nanopores under effects of adsorption,” *Chemical Engineering Journal*, vol. 419, p. 129625, 2021.
- [49] G. Cao, M. Lin, W. Jiang et al., “A statistical-coupled model for organic-rich shale gas transport,” *Journal of Petroleum Science and Engineering*, vol. 169, pp. 167–183, 2018.
- [50] B. L. Liu, A. Suzuki, and T. Ito, “Effect of capillary force on performance of shale rock fracturing,” *53rd US Rock Mechanics/Geomechanics Symposium*, 2019, New York City, June 2019, 2019.
- [51] G. Sheng, H. Zhao, Y. Su et al., “An analytical model to couple gas storage and transport capacity in organic matter with non-circular pores,” *Fuel*, vol. 268, p. 117288, 2020.
- [52] F. Javadpour, H. Singh, A. Rabbani, M. Babaei, and S. Enayati, “Gas flow models of shale: a review,” *Energy & Fuels*, vol. 35, no. 4, pp. 2999–3010, 2021.
- [53] W. Song, J. Yao, K. Zhang, H. Sun, and Y. Yang, “The impacts of pore structure and relative humidity on gas transport in shale: a numerical study by the image-based multi-scale pore network model,” *Transport in Porous Media*, pp. 1–25, 2021.
- [54] Z. Yi, S. Hu, S. Wu, J. Ma, J. Gao, and Y. Yuan, “Pore network extraction for shale gas flow in nanoporous media,” *Marine and Petroleum Geology*, vol. 126, p. 104896, 2021.
- [55] Z. Sun, J. Shi, K. Wu et al., “Transport capacity of gas confined in nanoporous ultra-tight gas reservoirs with real gas effect and water storage mechanisms coupling,” *International Journal of Heat and Mass Transfer*, vol. 126, pp. 1007–1018, 2018.

- [56] R. Xu, M. S. Prodanović, and C. J. Landry, "Simulation of gas adsorption and capillary condensation in shale Nanopores using lattice Boltzmann modeling," in *SPE/AAPG/SEG Unconventional Resources Technology Conference*, Houston, Texas, USA, July 2018.
- [57] Z. Song, Y. Song, J. Guo, Z. Zhang, and J. Hou, "Adsorption induced critical shifts of confined fluids in shale nanopores," *Chemical Engineering Journal*, vol. 385, p. 123837, 2020.
- [58] F. Javadpour, D. Fisher, and M. Unsworth, "Nanoscale gas flow in shale gas sediments," *Journal of Canadian Petroleum Technology*, vol. 46, no. 10, 2007.
- [59] B. Hu and J. G. Wang, "A lattice Boltzmann simulation on the gas flow in fractal organic matter of shale gas reservoirs," *Journal of Petroleum Science and Engineering*, vol. 210, p. 110048, 2022.
- [60] Y. Li, P. Dong, and D. Zhou, "A dynamic apparent permeability model for shale microfractures: coupling poromechanics, fluid dynamics, and sorption-induced strain," *Journal of Natural Gas Science and Engineering*, vol. 74, p. 103104, 2020.
- [61] Z. Liehui, S. Baochao, Z. Yulong, and G. Zhaoli, "Review of micro seepage mechanisms in shale gas reservoirs," *International Journal of Heat and Mass Transfer*, vol. 139, pp. 144–179, 2019.
- [62] S. Zhan, Y. Su, Z. Jin, W. Wang, and L. Li, "Oil-water two-phase flow behavior in shale inorganic nanopores: from molecule level to theoretical mathematical model," in *Unconventional Resources Technology Conference*, December 2020.
- [63] N. Sobacki, C. Nieto-Draghi, A. Di Lella, and D. Y. Ding, "Phase behavior of hydrocarbons in nano-pores," *Fluid Phase Equilibria*, vol. 497, pp. 104–121, 2019.
- [64] C. Herdes, C. Petit, A. Mejia, and E. A. Muller, "Combined experimental, theoretical, and molecular simulation approach for the description of the fluid-phase behavior of hydrocarbon mixtures within shale rocks," *Energy & Fuels*, vol. 32, no. 5, pp. 5750–5762, 2018.
- [65] S. Luo, J. Lutkenhaus, and H. Nasrabadi, "A framework for incorporating nanopores in compositional simulation to model the unusually high GOR observed in shale reservoirs," *SPE Reservoir Simulation Conference*, 2019, Galveston, Texas, USA, 2019, 2019.
- [66] X. Zheng, B. Zhang, H. Sanei et al., "Pore structure characteristics and its effect on shale gas adsorption and desorption behavior," *Marine and Petroleum Geology*, vol. 100, pp. 165–178, 2019.
- [67] K. Zeng, P. Jiang, Z. Lun, and R. Xu, "Molecular simulation of carbon dioxide and methane adsorption in shale organic nanopores," *Energy & Fuels*, vol. 33, no. 3, pp. 1785–1796, 2019.
- [68] K. Zhang, L. Liu, and G. Huang, "Nanoconfined water effect on CO₂ utilization and geological storage," *Geophysical Research Letters*, vol. 47, no. 15, p. e2020GL087999, 2020.
- [69] K. Zhang, N. Jia, S. Li, and L. Liu, "Quantification and evaluation of thermodynamic miscibility in nanoconfined space," *Industrial & Engineering Chemistry Research*, vol. 58, no. 11, pp. 4609–4624, 2019.
- [70] D. Feng, S. Bakhshian, K. Wu et al., "Wettability effects on phase behavior and interfacial tension in shale nanopores," *Fuel*, vol. 290, p. 119983, 2021.
- [71] K. Zhang, N. Jia, and L. Liu, "CO₂ storage in fractured nanopores underground: phase behaviour study," *Applied Energy*, vol. 238, pp. 911–928, 2019.
- [72] J. Xie, M. K. Borg, L. Gibelli, O. Henrich, D. A. Lockerby, and J. M. Reese, "Effective mean free path and viscosity of confined gases," *Physics of Fluids*, vol. 31, no. 7, article 072002, 2019.
- [73] D. Chai, Z. Fan, and X. Li, "A new unified gas-transport model for gas flow in nanoscale porous media," *SPE Journal*, vol. 24, no. 2, pp. 698–719, 2019.
- [74] M. He, Y. Zhou, B. Chen et al., "Effect of pore structure on slip-page effect in unsaturated tight formation using pore network model," *Energy & Fuels*, vol. 35, no. 7, pp. 5789–5800, 2021.
- [75] G. Karniadakis, A. Beskok, and N. Aluru, *Microflows and Nanoflows: Fundamentals and Simulation*, Springer Science & Business Media, 2006.
- [76] K. Wu, Z. Chen, X. Li, C. Guo, and M. Wei, "A model for multiple transport mechanisms through nanopores of shale gas reservoirs with real gas effect-adsorption-mechanic coupling," *International Journal of Heat and Mass Transfer*, vol. 93, pp. 408–426, 2016.
- [77] K. Wu, X. Li, C. Wang, W. Yu, and Z. Chen, "Model for surface diffusion of adsorbed gas in nanopores of shale gas reservoirs," *Industrial & Engineering Chemistry Research*, vol. 54, no. 12, pp. 3225–3236, 2015.
- [78] W. Pang and Z. Jin, "Ono-Kondo lattice model for propane multilayer adsorption in organic nanopores in relation to shale gas," *Fuel*, vol. 235, pp. 158–166, 2019.
- [79] G. Sheng, Y. Su, F. Javadpour et al., "New slip coefficient model considering adsorbed gas diffusion in shale gas reservoirs," *Energy & Fuels*, vol. 34, no. 10, pp. 12078–12087, 2020.
- [80] S. Alafnan, A. Awotunde, G. Glatz, S. Adjei, I. Alrumaih, and A. Gowida, "Langmuir adsorption isotherm in unconventional resources: applicability and limitations," *Journal of Petroleum Science and Engineering*, vol. 207, p. 109172, 2021.
- [81] S. Huang, Y. Wu, L. Cheng, H. Liu, Y. Xue, and G. Ding, "Apparent permeability model for shale gas reservoirs considering multiple transport mechanisms," *Geofluids*, vol. 2018, 18 pages, 2018.
- [82] S. K. Loyalka and S. A. Hamoodi, "Poiseuille flow of a rarefied gas in a cylindrical tube: solution of linearized Boltzmann equation," *Physics of Fluids A*, vol. 2, no. 11, pp. 2061–2065, 1990.
- [83] S. A. Tison, "Experimental data and theoretical modeling of gas flows through metal capillary leaks," *Vacuum*, vol. 44, no. 11–12, pp. 1171–1175, 1993.
- [84] E. R. Gilliland, R. F. Baddour, G. P. Perkinson, and K. J. Sladek, "Diffusion on surfaces. I. Effect of concentration on the diffusivity of physically adsorbed gases," *Industrial and Engineering Chemistry Fundamentals*, vol. 13, no. 2, pp. 95–100, 1974.
- [85] Y. T. Yeh, *Diffusion and Adsorption of Gases in Molecular Sieves (PhD Diss.)*, State University of New York, Buffalo, 1989.
- [86] D. M. Ruthven and K. F. Loughlin, "Correlation and interpretation of zeolitic diffusion coefficients," *Transactions of the Faraday Society*, vol. 67, pp. 1661–1671, 1971.
- [87] D. Liu, H. Ge, Y. Shen, H. Liu, and Y. Zhang, "Experimental investigation on imbibition characteristics of shale with highly developed bedding fractures," *Journal of Natural Gas Science and Engineering*, vol. 96, p. 104244, 2021.
- [88] M. Arif, M. Mahmoud, Y. Zhang, and S. Iglauer, "X-ray tomography imaging of shale microstructures: a review in the context of multiscale correlative imaging," *International Journal of Coal Geology*, vol. 233, p. 103641, 2021.